ACS APPLIED MATERIALS & INTERFACES

Research Article

www.acsami.org

Polarization-Sensitive Linear Plasmonic Nanostructures via Colloidal Lithography with Uniaxial Colloidal Arrays

V. Saracut,[†] M. Giloan,[†] M. Gabor,[‡] S. Astilean,*[,†] and C. Farcau*[,†]

[†]Nanobiophotonics and Laser Microspectroscopy Centre, Institute for Interdisciplinary Research in Bio-Nano-Sciences, and Faculty of Physics, Babes-Bolyai University, 42 T. Laurian Street, 400271 Cluj-Napoca, Romania

[‡]Center for Superconductivity, Spintronics and Surface Science, Technical University of Cluj-Napoca, 28 Memorandumului Street, RO-400114 Cluj-Napoca, Romania

Supporting Information

ABSTRACT: The ability of metallic nanostructures to support surface plasmon excitations is widely exploited nowadays for developing new technologies and applications in many fields, like communications, medicine or environment. It is known that the plasmonic response of a nanostructure is strongly dependent on its size and shape, and thus a fine control of these features is required for developing applications. In this paper uniaxial colloidal crystal arrays are prepared by convective self-assembly on DVD surfaces. These are then used as template/mask for metal film deposition, in order to obtain two original kinds of metallic nanostructures with controllable morphology: (i) linear arrays of metal half-shells (LAMHSs) and (ii) arrays of periodically serrated plasmonic strips (PSPSs). Angle-resolved optical transmittance measurements reveal the presence of several surface plasmon resonances, while polarized light transmission demonstrates the anisotropic plasmonic response of both LAMHSs and PSPSs. FDTD simulations support the experimental observations and help in the assignments of observed plasmon modes. The proposed linear metallic nanostructures can prove useful for the design of plasmonic components.

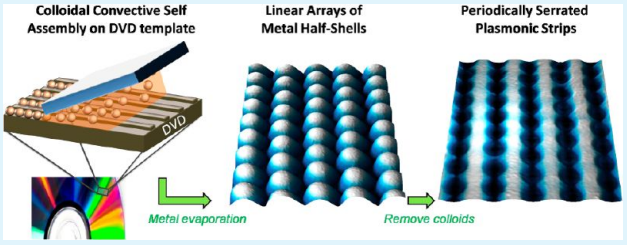

KEYWORDS: *convective self-assembly, DVD, colloidal crystals, half-shells, metallic strips, surface plasmons, polarizer*

1. INTRODUCTION

Nanostructured materials continue to attract interest due to their unique properties and applications which are different from those of bulk materials. Noble metal nanostructures are a special class of nanomaterials that are well-known for their extraordinary optical properties.[1,2] These arise from surface plasmon resonances, collective oscillations of their conduction electrons as a response to an optical electric field. The development of new devices and applications which benefit from the plasmonic properties of metallic nanostructures is closely related to the ability to control a number of parameters such as size, shape, dielectric properties of both the material and the surrounding medium.[2−5] Applications of metallic nanostructures include optical filters, probes for scanning near-field optical microscopy, nanoscale waveguides, and photon energy transport devices,[1,2,6−8] active surfaces for surface-enhanced spectroscopic techniques and chemical or biological optical sensors.[9−14] Many methods of fabricating plasmonic nanostructures have been recently developed, such as chemical synthesis, template-directed growth, and lithographic techniques.[2,10] Among these techniques, electron beam lithography[15] and focused ion beam lithography[16] offer a precise control over the placement, size, and shape of metallic nanostructures but are in general complex, expensive, and require highly specialized facilities. Several nonconventional lithographic techniques have also been proposed, including those based on colloidal crystals obtained by self-assembly, which are then used as masks or templates for the deposition or growth of metallic films. By simply evaporating a metallic film on top of monolayer hexagonal-packed colloidal crystals one can obtain periodic 3D-like structures, such as arrays of half-shells or bowls.[17,18] These possess very attractive optical properties, dominated by complex plasmonic-photonic interactions in the hybrid metal-dielectric periodic structure, which can be tuned by the colloidal sphere diameter and thickness of metal film.[19,20] The particular case of nanosphere lithography (NSL),[21,22] involves a supplementary step of colloidal sphere removal, such that a periodic array of triangular-shaped nanoparticles is obtained on the substrate. The 2D arrays of colloidal spheres (usually polystyrene or silica) can be obtained by evaporation-induced self-assembly strategies. Such a technique is convective self-assembly (CSA),[23−25] which is based on convective flow of particles in a colloidal suspension toward the triple-contact line where they assemble by capillary forces. One can obtain by this method large areas (several cm^2) of compact colloidal crystal monolayers. However, these colloidal monolayers, besides being of a given hexagonal lattice symmetry, they are polycrystalline, with many defects and

Received: November 12, 2012
Accepted: January 22, 2013
Published: January 22, 2013

   dx.doi.org/10.1021/am3026745 | ACS Appl. Mater. Interfaces 2013, 5, 1362−1369

different crystal orientations. These are all inconveniences toward the control of the optical properties of the resulting metallic nanostructures. There are some reports in which, by performing CSA on topographically patterned surfaces, colloidal lattices with good control over crystal orientation were produced.[23,24,26] However the number of reports on plasmonic nanostructures fabricated with such well-controlled colloidal arrays is very limited.

In this work, we report a simple method to fabricate parallel, uniaxial arrays of polystyrene spheres employing convective self-assembly on highly available and inexpensive DVD surfaces as templates. These Uni-Axial Colloidal Arrays (UACAs) are then used as lithographic masks to produce two kinds of original metal nanostructures: linear arrays of metal half shells (LAMHSs), and periodically serrated plasmonic strips (PSPSs). Their morphology is analyzed by scanning electron microscopy and atomic force microscopy. The transmission properties are analyzed with respect to incident angle and direction of polarization with respect to the linear nanostructures. FDTD simulations are performed, which help identify some of the surface plasmon modes dominating the optical response.

2. MATERIALS AND METHODS

2.1. Materials. Polystyrene spheres with 500 nm diameter in aqueous suspension (2% W/v) were purchased from microparticles GmbH. Suspensions of desired concentration were prepared by dilution with distilled water, which were then used for convective assembly.

The inner surface of a Digital Versatile Disc (DVD) was used as substrate. The DVD structure consists of two polycarbonate discs, one of them being inscribed with a channel spiraling from its center to its periphery, a thin metallic film as a reflecting layer and a dye-containing layer as the recording medium sandwiched between the discs. The two discs were mechanically separated, and samples of rectangular shape were cut from the periphery of the DVD. In this region the grooves (750 nm period and 100 nm depth) can be approximated as parallel over a length of several millimeters (see sketch in Figure 1a and Figure S1 of the Supporting Information). The metallic foil was removed by adhesive tape and the dye was washed by rinsing several times with isopropanol. Undesired remains of metal and dye were removed by sonication. After rinsing with distilled water, the surface was dried followed by 20 min treatment in a Novascan PSD PRO-UV UV ozone system to render the surface hydrophilic.

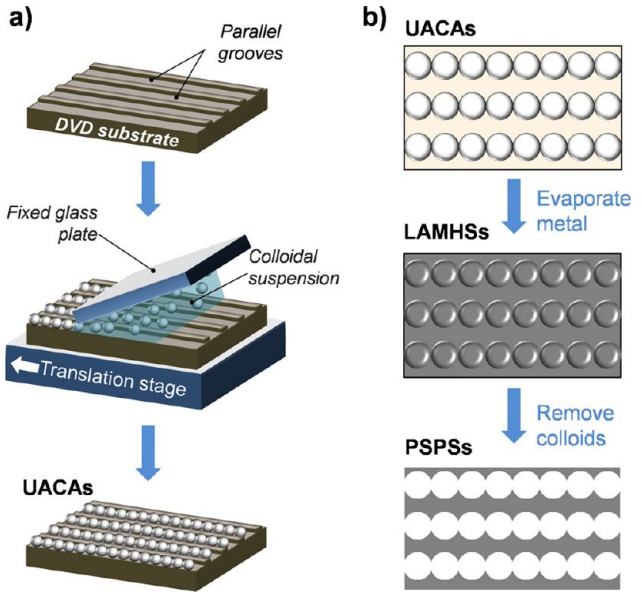

Figure 1. Schemes depicting: (a) preparation of uniaxial colloidal arrays (UACAs) by convective self-assembly on DVD surface; (b) fabrication of linear arrays of metallic half-shells (LAMHSs) and arrays of periodically serrated plasmonic strips (PSPSs) by colloidal lithography with UACAs.

2.2. Colloidal Assembly on DVD. Polystyrene spheres were deposited on the prepared DVD substrate by convective self-assembly. The whole process is schematized in Figure 1a. The DVD substrate was fixed on a horizontal motorized translation stage, controlled through computer software. A rectangular glass plate was attached to a pole at an angle of about 25°, such that one of its edges comes near the substrate parallel to it and perpendicular to the array of channels on the DVD substrate. A 5 to 7 μL drop of colloidal suspension was inserted into the wedge formed by the glass plate and the DVD substrate. The stage was then translated relative to the fixed glass plate with a desired speed along a direction parallel to the substrate channels (see Figure 1a). The process took place in ambient conditions (30−32 °C and 28−34%RH). Colloidal suspension concentration used was 0.33% W/v and the speed at which the substrate was translated ranged between 4 and 7μm/s.

2.3. Fabrication of Metal Nanostructures. A thin film of silver was deposited on the prepared Uni-Axial Colloidal Arrays (UACAs) by means of vacuum thermal evaporation at normal or oblique incidence, as specified later. Film thickness was monitored by a quartz crystal microbalance, to about 50 nm on all the samples discussed here. On some of these metal-coated samples, the polystyrene spheres with their metallic caps were removed using adhesive tape, to reveal the metallic structures formed on the substrate.

2.4. Characterization Techniques. Optical microscopy, scanning electron microscopy (SEM) on a Quanta 3D FEG-FEI and atomic force microscopy (AFM) on a WITec system were employed for samples characterization. Optical transmission measurements in nonpolarized light were made with an Ocean Optics USB4000 UV−vis system equipped with two QP100−2-VIS/BX optical fibers of 100 μm core diameter. The ends of the optical fibers were placed at about 6 cm from each other and the sample was mounted between them in a collimated beam. The optical spot area on the sample was about 1 mm^2. The angle of incidence of light on the sample was varied in steps of two degrees. Polarized light transmission measurements were performed on an inverted Olympus optical microscope. A 10× objective and an optical fiber with 0.6 mm core diameter were used for collection, which reduces the analyzed sample area to a disk of approximately 60 μm diameter, and assures a negligible amount of scattered/diffracted light being collected.

2.5. Electromagnetic Simulations. Three-dimensional finite differences time domain (3D-FDTD) simulations have been performed in order to confirm the experimental results and to get insights of the optical properties of the fabricated materials. The geometry of the simulated nanostructures is described in detail in the Supporting Information, Figure S8. Refractive indexes of 1.578 and 1.585 have been considered for the substrate and spheres respectively. Silver permittivity and permeability used in simulations are described by the CRC values[27] provided by the software material database.[28] Appropriate periodic boundary conditions (PBC) were imposed on the edge planes of the simulation area perpendicular to y and z axes, and absorbing boundary conditions (ABC) were imposed on the edge planes of the simulation area perpendicular to x axis. Both materials were normally illuminated from the silver film side by plane waves (i.e., propagation direction parallel to x axis) with wavelengths in the range of 350−950 nm. Transmission spectra have been calculated for polarizations parallel to y and z axes. The real part of E_x component of the electric field was calculated on three monitoring planes xy, xz, and yz depicted in Figure S8 of the Supporting Information.

3. RESULTS AND DISCUSSION

3.1. Convective Self-Assembly on DVD Pattern. As shown in Figure 1, the colloidal drop is held between the DVD substrate and the deposition plate by capillary forces. Water

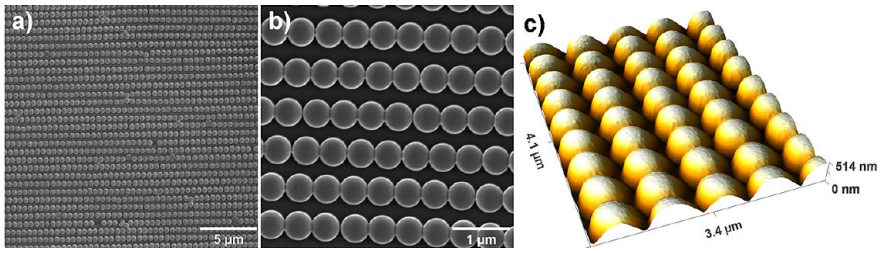

Figure 2. (a, b) SEM images of uniaxial colloidal arrays (UACAs), and (c) AFM image of linear arrays of metal half-shells (LAMHSs).

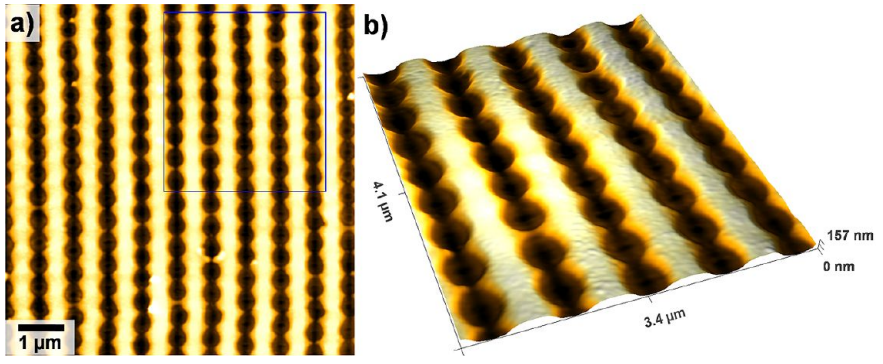

Figure 3. (a) AFM image of an array of periodically serrated plasmonic strips (PSPSs). (b) 3D zoom on the area marked by the rectangle in a.

begins to evaporate and a continuous flow compensates the evaporation, transporting colloidal polystyrene spheres to the meniscus (the triple contact line between substrate, colloid drop and air) where they are assembled. When the water film thickness is comparable to the particle diameter, attractive capillary forces are generated between the particles, which drive the packing process. If the substrate is flat, particles will assemble in layers with compact hexagonal arrangement.[23−25] Dimitrov and Nagayama[29] proposed a simple equation which describes the solvent flux and the accumulation of particles in the drying region. This shows that controlling three major process parameters (substrate velocity, colloid concentration, and solvent evaporation rate) one can control the thickness and structure of the coating.

In this work our goal was to arrange polystyrene spheres of 500 nm diameter along the DVD channels having 100 nm depth and a 750 nm spacing by CSA. The SEM images in Figure 2a and 2b present the typical results of the assembly process. The polystyrene spheres are well arranged along the substrate channels yielding an array of parallel colloidal chains, with a controlled preferential orientation, i.e., a uniaxial colloidal array (UACA). Monocrystalline regions with area of 2−3 mm^2 were obtained. However some defects are always present, such as interruptions of the colloidal chains, some overlapping spheres, or a few spheres of other sizes then the nominal 500 nm size (see Figure 2a). Note also that in the direction perpendicular to the colloidal chains there is no correlation between the spheres' positions. The density of colloids on the surface is smaller than that of a close-packed monolayer roughly by a factor of 1.6.

The assembly process is driven by the water convective flux, and the channels on the DVD substrate (oriented perpendicular to the meniscus) have the role of physically guiding along them the movement of the colloids brought toward the meniscus. The surface topography can modulate the shape of the meniscus, and possibly also the contact angle between the suspension and substrate varies spatially and can influence the result of the assembly process.[30] Then attractive capillary forces can arise both between adjacent particles in the same DVD groove, and between particles located in adjacent channels. Capillary forces between particles and lateral sides of the DVD grooves are not expected to contribute much to the ordering since the height of the grooves (∼100 nm) is much smaller than the sphere height (diameter ∼500 nm). The strength of the attraction capillary forces between adjacent spheres in the same channel is larger than those between colloids in adjacent channels, as this force is roughly inverse proportional with the interparticle distance.[31] Therefore conditions can be met that the system finds equilibrium and uniaxial arrays as those reported here are obtained. In our experiments, only the substrate velocity and the colloid concentration were controlled. An improved control over other process parameters such as substrate temperature, ambient temperature and humidity could lead to even larger areas of monocrystalline uniaxial colloidal arrays. Note that by covering the DVD surface with a compact packed monolayer of colloids, e.g., by increasing colloid concentration or reducing the deposition speed, some peculiar colloidal crystal arrays can be obtained, which deviate slightly from the perfect hexagonal lattice. Because of interference of the hexagonal array with the linear array on the substrate, some periodically distributed features result, examples of which are given in the Supporting Information.

3.2. Colloidal Lithography with Uniaxial Colloidal Arrays. The prepared UACAs constitute an interesting structure by itself, by similarity with the 2D hexagonal arrays which were shown to possess optical properties resulting from their periodicity,[32] as in photonic crystals. However we propose here the application of these UACAs as a template and mask for the fabrication of noble metal nanostructures. Silver was chosen as it is the metal with the best optical and surface plasmon properties (although it gets oxidized in air), and it allow one to map the optical response all across the visible spectrum. By depositing a thin film of silver (50 nm) over this colloidal crystal, a nanostructured surface consisting of aligned metal-

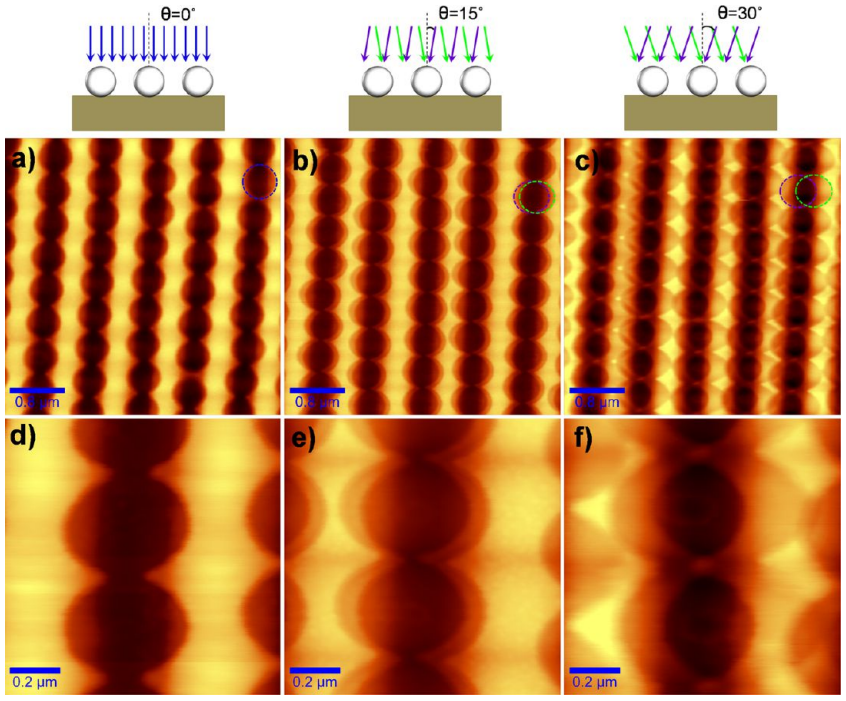

Figure 4. AFM images of arrays of periodically serrated plasmonic strips (PSPSs) obtained by oblique angle Ag film evaporation. PSPSs were obtained by (a, d) a single evaporation an normal incidence; (b, e) two evaporation steps, by angling the substrate with respect to the evaporation beam by +15° and −15°; (c, f) two steps, by angling the substrate by +30° and −30°. The circles indicate the shadow shed by a sphere on the substrate in each evaporation process.

coated spheres was obtained, referred here as linear arrays of metal half-shells (LAMHSs) (Figure 2c). Such a structure is similar to so-called metal films over nanospheres (MFON)[21,22] or hybrid plasmonic-photonic crystals,[33] which were demonstrated to possess interesting and highly tunable plasmonic properties but also applications as surface enhanced Raman scattering[21,34] or surface-enhanced fluorescence substrates.[12,13]

Furthermore, the evaporated metal is deposited both on top of the spheres and on the substrate through interstitial open spaces between the linear arrangements of spheres. By removing the polystyrene spheres with their metallic caps an interesting type of structure consisting of silver strips, laterally decorated with sawtooth-like periodic serrations can be obtained on the substrate, as schematized in Figure 1b. These structures will be referred to as periodically serrated plasmonic strips (PSPSs). Some AFM topographical images of the experimentally realized PSPSs are shown in Figure 3a and 3b. The sawtooth-like serrations are distributed along the edges of each metal strip, being equally spaced by 500 nm, the diameter of the polymer spheres. The apex of each "sawtooth" mirrors another tooth located on the adjacent strip. On the contrary, the teeth on one and the other side on a given metallic strip are noncorrelated, since their formation originates in different chains of polymer spheres, which as mentioned already are noncorrelated. The average distance between two mirroring apexes is around 100 nm. The sharp teeth on the silver strips are expected to be highly effective in amplifying and localizing electromagnetic fields, so desirable in the field of plasmonics, and necessary for controlling and manipulating plasmon-molecule interactions, as in surface enhanced Raman scattering or surface enhanced fluorescence. We also expect that due to their high aspect ratio (tens of micrometers length, tens to hundreds of nm width, and tens of nm height) these metallic periodically serrated strips could find potential in plasmonic waveguide applications, as the recently proposed plasmonic belts.[35]

It is known that although tips and apexes are efficient in electromagnetic field localization, pairs of such tips separated by very narrow gaps provide a strong boost of field enhancement, as shown for so-called bow-tie nanoantennas.[36] A controlled fabrication of large area arrays of such nanoscale gaps still represents an ongoing challenge. Following this idea we explored the possibility to approach the teeth on the fabricated silver strips, by a double evaporation and adjustment of the angle of film deposition. In standard metal film evaporation procedure, the sample is oriented perpendicular to the evaporating metal vapor beam and PSPSs as those shown in Figures 3, 4a, and 4d are obtained. The two-step procedure was performed as follows: in the first step the sample was rotated by an angle θ around an axis parallel to the colloidal chains, thus the evaporation beam makes an angle θ to the direction normal to the plane of the colloidal mask; 25 nm of silver were deposited; the second step is identical but the sample was rotated in the opposite direction, i.e., by an angle $-\theta$ (see sketch at the top of Figure 4).

By the two-step evaporation at angle θ = 15° the structure presented in Figure 4b, e was obtained. The sawtooth-like serrations indeed approach the pair serrations on the adjacent silver strip. The average distance between two mirroring apexes is around 30 nm. By further increasing θ to 30° the pairing serrations overlapped, and the resulting metal film is rather a complex 3D-like metal film with periodic linear arrays of perforations.

These results prove an interesting degree of tuning the morphology of these PSPSs. A fine manipulation of the deposition angle should make it possible to obtain very narrow metallic gaps, arrayed and oriented in a controlled fashion.

dx.doi.org/10.1021/am3026745 | ACS Appl. Mater. Interfaces 2013, 5, 1362−1369

3.3. Optical Response of LAMHSs. The morphology of these metal nanostructures, possessing a high aspect ratio and periodicity, suggests that their optical response should be sensitive to the polarization and angle of incident light. The optical properties of the prepared linear nanostructures were thus explored by transmission measurements. The angle-resolved unpolarized transmission spectra of LAMHSs are presented in Figure 5. Next the configuration of the angle-

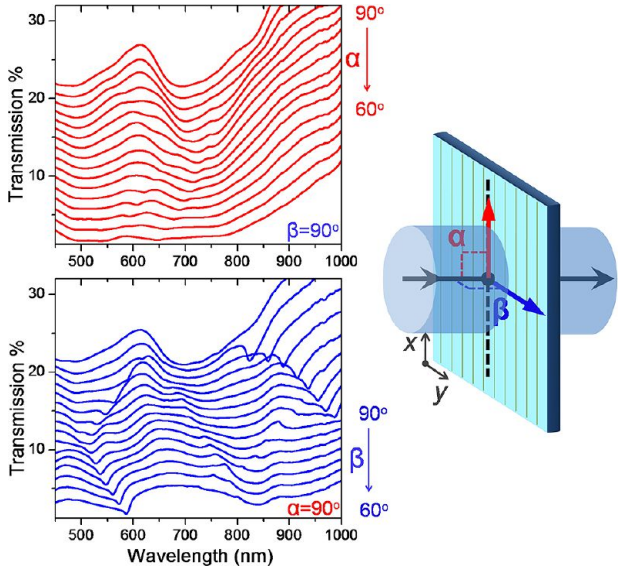

Figure 5. (Left) Angle-resolved unpolarized transmission spectra of linear arrays of silver half-shells. The individual spectra are offset vertically by 60% for clarity. (Right) Scheme showing the orientation of the incident light beam relative to the linear plasmonic nanostructures.

resolved measurements is briefly explained. Consider that the linear plasmonic nanostructures lie in the XY plane and their orientation is along the X axis (see scheme in Figure 5). At normal incidence the light beam makes an angle α with the X axis and an angle β with the Y axis which are equal to 90°. The angle of incident light relative to the sample surface was varied in two distinct ways: (1) angle α is decreased from 90° while angle β is maintained fixed at 90°; and (2) angle β is decreased from 90° while α is maintained at 90°.

Several observations can be made on the transmission spectra in Figure 5, as follows. The normal incidence spectrum presents a main broad transmission peak centered between 550 and 650 nm, a minimum between 700 and 800 nm and then an increase toward the NIR region. The transmission level is higher than that of a silver film having the same thickness (50 nm) deposited onto a bare DVD grating (not shown here). These transmission peaks suggest the excitation of different plasmonic modes which contribute to the increased transmission as it was demonstrated already for the hexagonal compact arrays of metallic half-shells,[37] and similar to the well-known Extraordinary Optical Transmission (EOT).[38] Different behaviors are observed by angle-resolved measurements, with the modification of either α or β as depicted in Figure 5a. Optical modes of different nature can be observed, which shift considerably either to shorter or to longer wavelengths when the angle of incidence is modified.

When either angle α or β is modified an increase in the in-plane component of incident light wavevector along or perpendicular to the axis of the plasmonic structures takes place. This in-plane wavevector component and the simultaneous increase of electric field component perpendicular to the plane can have multiple effects, like pure grating diffraction effects, coupling of light into propagative surface plasmon polaritons, or excitation of localized surface plasmon modes.

To exploit the linear morphology of the fabricated nanostructures polarized light transmission spectra were recorded. Figure 6 presents a selection of spectra recorded at

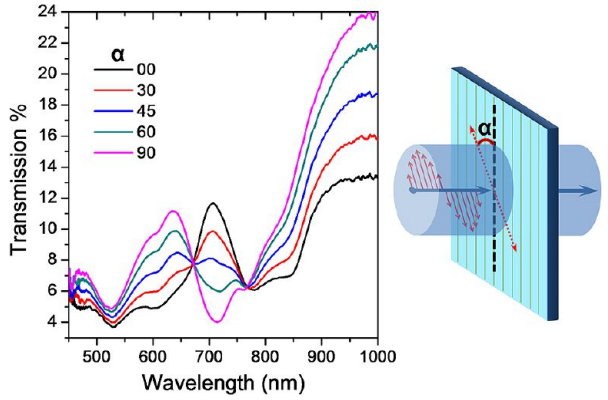

Figure 6. Polarized transmission spectra of linear arrays of silver half-shells. The angle between light polarization and the linear plasmonic structure is depicted in the scheme.

normal incidence, with the incident light polarization being rotated from a parallel alignment to a perpendicular alignment, with respect to the LAMHSs plasmonic structures. A very interesting observation concerns the spectral region between 500 and 800 nm. When light is polarized parallel to the linear silver nanostructures, a peak is observed around 700 nm, which is suppressed as the polarization rotates toward perpendicular configuration. Instead, another transmission maximum appears around 620 nm. These two peaks are separated by an isosbestic point located at 670 nm. Another isosbestic point is situated at 780 nm. Above it, the transmittance is also higher in the perpendicular configuration than in the parallel one. To understand the optical response and to make an assignment of the observed transmission peaks FDTD simulations were performed.

The computed transmittance spectra of LAMHSs are represented in Figure 7a, b (solid lines) for both parallel and perpendicular configuration at normal incidence. Generally a satisfactorily agreement between simulation and experiment was obtained with respect to both shape and spectral position of the observed features. When incident light is polarized parallel to the array of silver half-shells two transmission maxima are found while the experiment presents only one band. In Figure 7c the Ex component at one of these transmission maxima (670 nm, indicated by the solid arrow) is mapped in the plane containing the polarization (see the Supporting Information for a clear description) and sectioning the metal half-shells and spheres. This electric field distribution is identical to that previously found in hexagonal compact arrays of metal-coated spheres and attributed to a propagative surface plasmon mode originating in a guided mode observed also on bare dielectric sphere array.[37,39] In contrast with the previously investigated metal-coated hexagonal arrays, in the LAMHSs, this plasmon mode can be selectively excited by choosing the parallel polarization. The Ex distribution

dx.doi.org/10.1021/am3026745 | ACS Appl. Mater. Interfaces 2013, 5, 1362−1369

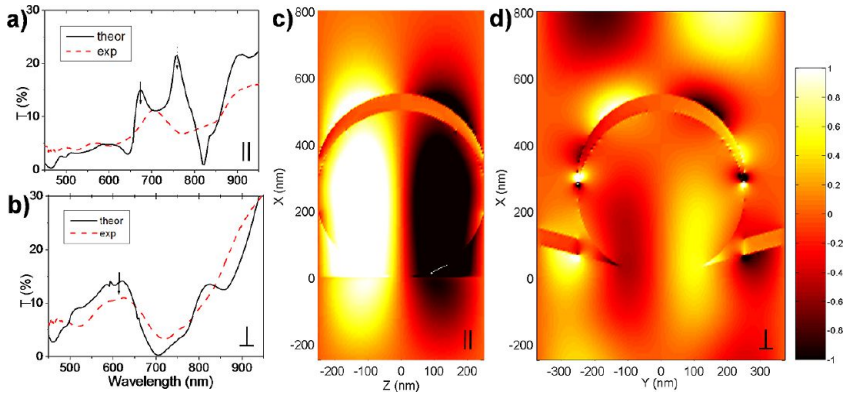

Figure 7. Transmission spectra computed by FDTD (solid lines) for: (a) incident polarization parallel to the LAMHSs; (b) incident polarization perpendicular to the LAMHSs; Experimental spectra (dotted lines) are included for comparison. (c) Map of the Ex component at 670 nm (indicated by the full arrow in a) in a vertical plane along the linear array of spheres and metal half-shells; (d) map of the Ex component at 611 nm (indicated by the solid arrow in b) in a plane perpendicular to the linear array of half-shells.

associated to the 760 transmittance maximum is quite similar and can be found in the Supporting Information. For perpendicular polarization, the Ex component at the transmission maximum shows a different pattern, with a more complex field distribution (Figure 7d). In this case, the transmission is probably realized by a strong scattering of the individual metal half-shells. Note that for the perpendicular polarization a better agreement is obtained between experiment and theory than for parallel polarization. We suggest this results from the imperfections of the array in the real samples: when light is polarized along the half-shells array, collective modes related to the linear periodic arrangement are excited, whereas for perpendicular polarization, rather single half-shell modes are excited.

3.4. Optical Response of PSPSs. Figure 8 presents the angle-resolved unpolarized transmission spectra of periodically serrated silver strips, obtained by normal incidence metal evaporation (see Figure 4a, d). Several transmission minima, which shift either to shorter or longer wavelengths with the modification of light beam incident angle, are observed. Modes that change energy with incident angle are generally related to propagative surface plasmon polariton modes or pure diffraction grating effect. However, different localized plasmon modes can be more efficiently excited when the incident angle changes, because of simultaneous change in the electric field component perpendicular to the surface. An example of such a mode which does not exhibit an important shift is that between 750 and 800 nm in the upper panel of Figure 8. For the PSPSs samples an important amount of nonmetalized, free substrate area is available through which light can be transmitted, thus we believe that transmission minima are indicative of plasmonic modes, either localized at the sharp teeth or propagating along the strip.

Polarized spectra of PSPSs are presented in Figure 9. Three isosbestic points at 610, 760, and 880 nm can be observed. In

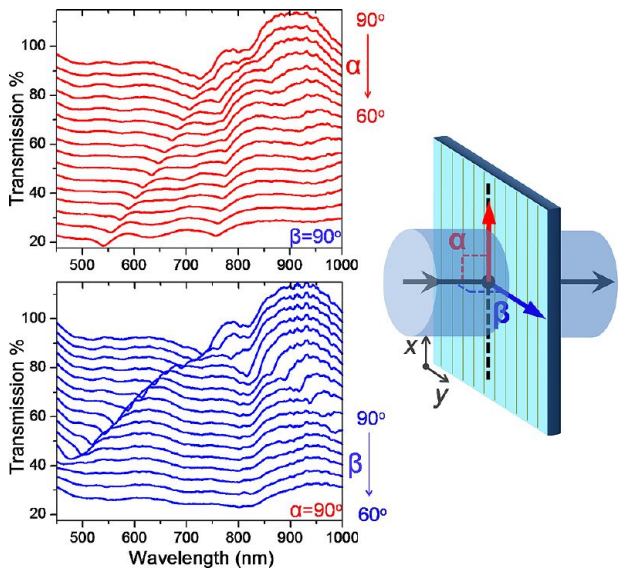

Figure 8. (Left) Nonpolarized angle-resolved transmission spectra on arrays of periodically serrated plasmonic strips. The individual spectra are offset vertically by 60% for clarity. (Right) Scheme showing the orientation of the incident light beam relative to the linear plasmonic nanostructures.

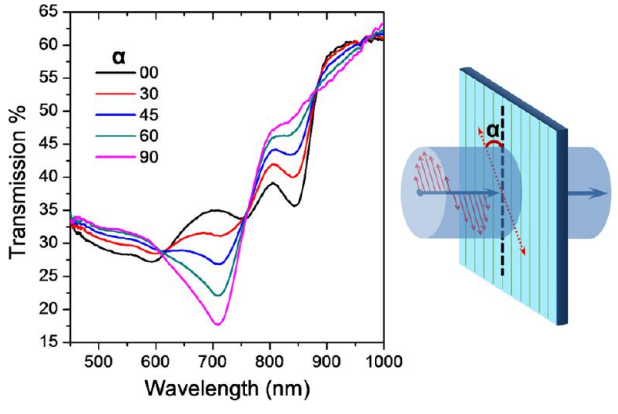

Figure 9. Polarized transmission spectra of PSPSs. The angle between light polarization and the linear plasmonic structure is depicted in the scheme.

the region between 610 and 760 the transmittance decreases, whereas in the 760−880 nm region, it increases when the polarization is rotated from parallel to perpendicular to the silver strips.

The computed transmittance spectra of PSPSs are represented in Figure 10a, b (solid lines) for light polarized parallel and perpendicular to the metal strips, at normal incidence. Again a generally good agreement between

dx.doi.org/10.1021/am3026745 | ACS Appl. Mater. Interfaces 2013, 5, 1362−1369

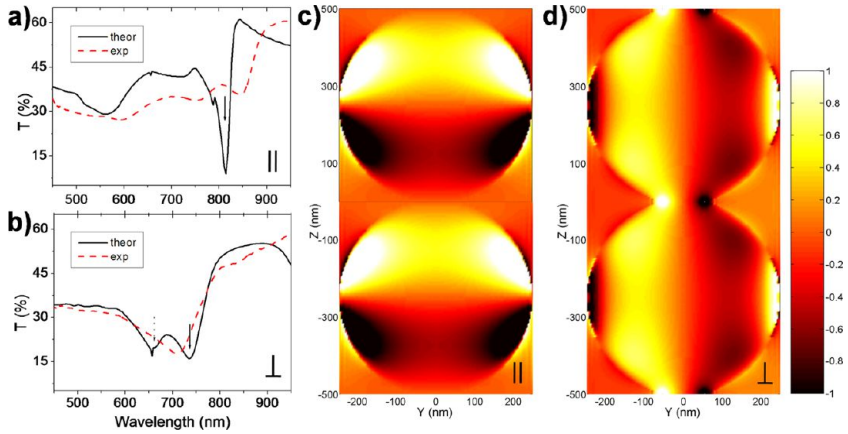

Figure 10. Transmission spectra of PSPS array computed by FDTD (solid lines) for: (a) incident polarization parallel to the PSPSs; (b) incident polarization perpendicular to the PSPSs; experimental spectra (dotted lines) are included for comparison. (c) Map of the Ex component at 737 nm (indicated by the solid arrow in a) in a vertical plane along the linear array of spheres and metal half-shells; (d) map of the Ex component at 813 nm (indicated by the full arrow in b) in a plane perpendicular to the linear array of half-shells.

simulation and experiment was obtained. When incident light is polarized parallel to the silver strips a narrow and deep minimum is observed at 813 nm, which in the experiment corresponds to a broader minimum at about 845 nm. In Figure 10c, the Ex component at the transmission minimum (813 nm, indicated by the solid arrow in Figure 10a) is mapped in a plane parallel to the sample "plane" (see the Supporting Information for a description). The electric field distribution suggests that a plasmon mode excited along the periodically corrugated edge of the metal strip is responsible for the observed transmission dip. For perpendicular polarization, the computed transmittance spectrum presents two overlapping minima, which coincide with the position of the broad minimum in the experimental spectrum. The map of the Ex component in the YZ plane (see the Supporting Information) at the 737 nm transmission minimum (solid arrow in Figure 10b) is shown in Figure 10d. Plasmon modes localized around the apexes of the 'teeth' are observed and probably also a mode related to grating coupling is superimposed. The second minimum, at 660, presents a similar Ex structure, but the supposed grating mode is missing (see Figure S9 in the Supporting Information). Again, a better agreement between experiment and theory is obtained for perpendicular polarization. It should be mentioned that there are several discrepancies between the geometry of the real samples and the simulated ones, especially in the case of PSPSs. The most important refers to the spatial positions of the sawtooth-like features located on one and the other side of a given strip, which are not correlated in the experiment, whereas in the simulation, a perfectly periodic lattice is considered.

The experimentally and theoretically observed behaviors suggest that the fabricated linear plasmonic nanostructures could find use as polarization-sensitive plasmonic components, as for example commutable band-pass filters in the case of LAMHSs. Although the transmittance is kind of low and improvements are needed, the structure could prove interesting. Note also that colloidal spheres with 500 nm diameter were chosen in order to match well with the 750 nm period of the DVD pattern, from the point of view of the colloidal assembly process. However, preliminary results suggest that spheres of other diameters, both smaller and larger (350 and 700 nm) could be used (see the Supporting Information for a discussion on this topic). This would allow for an important tunability of the polarization-sensitive optical/plasmonic response of both LAMHSs and PSPSs. To identify all the surface plasmon modes involved and the subtleties of their optical response further theoretical work is needed, task beyond the purpose of the present paper. However, these preliminary results represent a motivation to carry on the study of the optical properties of these types of noble metal plasmonic nanostructures, in the same time highlighting their applicative and fundamental scientific potential.

4. CONCLUSIONS

Linear array of polystyrene spheres were fabricated by convective self-assembly using the grooves on a DVD surface as topographical template. These uniaxial colloidal crystals were then used to obtain noble metal nanostructures: linear arrays of metal half shells (LAMHSs) and periodically serrated plasmonic strips (PSPSs). The analysis of their optical transmission properties indicates that these linear plasmonic nanostructures support the excitation of surface plasmon polaritons, while angle-resolved measurements highlight the presence of highly dispersive plasmonic modes. Their anisotropic optical response is evidenced by polarized transmission measurements, and also by FDTD simulations. Specifically, the LAMHSs can contribute to attain better control and manipulation of the surface plasmon enhanced electromagnetic fields in hybrid plasmonic-photonic crystals, like the previously studied metal-coated colloidal lattices.[33,37] The PSPSs, metallic strips with periodically corrugated edges, represent a new class of plasmonic materials, with potential in plasmon-enhanced spectroscopies or plasmon waveguiding. Moreover, due to their shape asymmetry and controlled orientation, both types of nanostructures can be expected to serve in developing polarization-sensitive plasmonic components. Applications to polarized surface enhanced Raman scattering or directional control of emission through plasmon-enhanced fluorescence can also be envisaged.

■ ASSOCIATED CONTENT

Supporting Information

Information regarding the DVD pattern topography. Examples of colloidal compact monolayer arrangements obtained by CSA on DVD pattern surface. Results on the assembly of spheres of different diameters on DVD. Geometry of the simulated

structures and electric field maps. This material is available free of charge via the Internet at http://pubs.acs.org.

AUTHOR INFORMATION

Corresponding Author

*E-mail: simion.astilean@phys.ubbcluj.ro (S.A.); cosmin.farcau@phys.ubbcluj.ro (C.F.).

Notes

The authors declare no competing financial interest.

ACKNOWLEDGMENTS

This work was supported by a grant of the Romanian National Authority for Scientific Research, CNCS – UEFISCDI, Project PN-II-RU-TE-2011-3-0134. The authors thank O. Ponta and A. Vulpoi for support on SEM imaging.

REFERENCES

(1) Lindquist, N. C.; Nagpal, P.; McPeak, K. M.; Norris, D. J.; Oh, S.-H. *Rep. Prog. Phys.* **2012**, *75*, 036501.
(2) Rycenga, M.; Cobley, C. M.; Zeng, J.; Li, W.; Moran, C. H.; Zhang, Q.; Qin, D.; Xia, Y. *Chem. Rev.* **2011**, *111*, 3669−3712.
(3) González, A. L.; Noguez, C. *J. Comput. Theor. Nanosci.* **2007**, *4*, 231−238.
(4) Noguez, C. *J. Phys. Chem. C* **2007**, *111*, 3806−3819.
(5) Kelly, K. L.; Coronado, E.; Zhao, L. L.; Schatz, G. C. *J. Phys. Chem. B* **2003**, *107*, 668−677.
(6) Maier, S. A.; Brongersma, M. L.; Kik, P. G.; Meltzer, S.; Requicha, A. A. G.; Koel, B. E.; Atwater, H. A. *Adv. Mater.* **2003**, *15*, 562−562.
(7) Maier, S. A.; Atwater, H. A. *J. Appl. Phys.* **2005**, *98*, 011101−10.
(8) Ozbay, E. *Science* **2006**, *311*, 189−193.
(9) Willets, K. A.; Van Duyne, R. P. *Annu. Rev. Phys. Chem.* **2007**, *58*, 267−297.
(10) Fan, M.; Andrade, G. F. S.; Brolo, A. G. *Anal. Chim. Acta* **2011**, *693*, 7−25.
(11) Stuart, D. A.; Yuen, J. M.; Shah, N.; Lyandres, O.; Yonzon, C. R.; Glucksberg, M. R.; Walsh, J. T.; Van Duyne, R. P. *Anal. Chem.* **2006**, *78*, 7211−7215.
(12) Farcau, C.; Astilean, S. *Appl. Phys. Lett.* **2009**, *95*, 193110.
(13) Stranik, O.; McEvoy, H. M.; McDonagh, C.; MacCraith, B. D. *Sens. Actuators, B* **2005**, *107*, 148−153.
(14) Grande, M.; Bianco, G. V.; Vincenti, M. A.; Stomeo, T.; de Ceglia, D.; De Vittorio, M.; Petruzzelli, V.; Scalora, M.; Bruno, G.; D'Orazio, A. *Appl. Phys. Lett.* **2012**, *101*, 111606.
(15) Vieu, C.; Carcenac, F.; Pépin, A.; Chen, Y.; Mejias, M.; Lebib, A.; Manin-Ferlazzo, L.; Couraud, L.; Launois, H. *Appl. Surf. Sci.* **2000**, *164*, 111−117.
(16) MoberlyChan, W. J.; Adams, D. P.; Aziz, M. J.; Hobler, G.; Schenkel, T. *MRS Bull.* **2007**, *32*, 424−432.
(17) Love, J. C.; Gates, B. D.; Wolfe, D. B.; Paul, K. E.; Whitesides, G. M. *Nano Lett.* **2002**, *2*, 891−894.
(18) Liu, J.; Maaroof, A. I.; Wieczorek, L.; Cortie, M. B. *Adv. Mater.* **2005**, *17*, 1276−1281.
(19) Farcau, C.; Astilean, S. *J. Opt. A−Pure Appl. Opt.* **2007**, *9*, S345−S349.
(20) Zhan, P.; Wang, Z. L.; Dong, H.; Sun, J.; Wu, J.; Wang, H.-T.; Zhu, S. N.; Ming, N. B.; Zi, J. *Adv. Mater.* **2006**, *18*, 1612−1616.
(21) Zhang, X.; Yonzon, C. R.; Van Duyne, R. P. *J. Mater. Res.* **2006**, *21*, 1083−1092.
(22) Haynes, C. L.; Van Duyne, R. P. *J. Phys. Chem. B* **2001**, *105*, 5599−5611.
(23) Zhang, J.; Li, Y.; Zhang, X.; Yang, B. *Adv. Mater.* **2010**, *22*, 4249−4269.
(24) Malaquin, L.; Kraus, T.; Schmid, H.; Delamarche, E.; Wolf, H. *Langmuir* **2007**, *23*, 11513−11521.
(25) Prevo, B. G.; Velev, O. D. *Langmuir* **2004**, *20*, 2099−2107.
(26) Dziomkina, N. V.; Vancso, G. J. *Soft Matter.* **2005**, *1*, 265−279.
(27) *CRC Handbook of Chemistry and Physics*, 92nd ed.; Haynes, W. M., Ed.; CRC Press: Boca Raton, FL, 2011.
(28) *FDTD Solutions*; Lumerical Solutions, Inc.: Vancouver, BC; http://www.lumerical.com/.
(29) Dimitrov, A. S.; Nagayama, K. *Langmuir* **1996**, *12*, 1303−1311.
(30) Kumar, G.; Prabhu, K. N. *Adv. Colloid Interf.* **2007**, *133*, 61−89.
(31) Járai-Szabó, F.; Néda, Z.; Astilean, S.; Farcau, C.; Kuttesch, A. *Eur. Phys. J. E* **2007**, *23*, 153−159.
(32) Miyazaki, H.; Ohtaka, K. *Phys. Rev. B* **1998**, *58*, 6920−6937.
(33) Romanov, S. G.; Korovin, A. V.; Regensburger, A.; Peschel, U. *Adv. Mater.* **2011**, *23*, 2515−2533.
(34) Jensen, T. R.; Malinsky, M. D.; Haynes, C. L.; Van Duyne, R. P. *J. Phys. Chem. B* **2000**, *104*, 10549−10556.
(35) Anderson, L. J. E.; Payne, C. M.; Zhen, Y.-R.; Nordlander, P.; Hafner, J. H. *Nano Lett.* **2011**, *11*, 5034−5037.
(36) Ding, W.; Bachelot, R.; Kostcheev, S.; Royer, P.; Espiau de Lamaestre, R. *J. Appl. Phys.* **2010**, *108*, 124314.
(37) Farcau, C.; Giloan, M.; Vinteler, E.; Astilean, S. *Appl. Phys. B* **2012**, *106*, 849−856.
(38) Ebbesen, T. W.; Lezec, H. J.; Ghaemi, H. F.; Thio, T.; Wolff, P. A. *Nature* **1998**, *391*, 667−669.
(39) Landstrom, L.; Brodoceanu, D.; Bauerle, D.; Garcia-Vidal, F. J.; Rodrigo, S. G.; Martin-Moreno, L. *Opt. Express* **2009**, *17*, 761−772.